BOUNDARY LAYER, SKIN FRICTION, AND BOATTAIL PRESSURE MEASUREMENTS FROM THE YF-12 AIRPLANE AT MACH NUMBERS UP TO 3

David F. Fisher
Dryden Flight Research Center

SUMMARY

In-flight measurements of boundary layer and skin friction data were made on YF-12 airplanes for Mach numbers between 2.0 and 3.0. Boattail pressures were also obtained for Mach numbers between 0.7 and 3.0 with Reynolds numbers up to 4×10^8.

Boundary layer data measured along the lower fuselage centerline indicate local displacement and momentum thicknesses can be much larger than predicted, suggesting the need for careful consideration when integrating engine inlets and cooling air intakes into a supersonic cruise design.

Skin friction coefficients measured at two of five lower fuselage stations were significantly less than predicted by flat plate theory. Since other recent experiments have found local skin friction coefficients on the upper fuselage surface to be higher than predicted, it appears that the flat plate theory may not necessarily provide accurate, full-scale, localized skin friction predictions for supersonic cruise conditions. However, such compensating effects may be a forgiving factor when model to full-scale adjustments are made on the basis of the usual two-dimensional, flat plate relations.

The presence of large differences between measured boattail pressure drag and values calculated by a potential flow solution indicates the presence of vortex effects on the upper boattail surface. At both subsonic and supersonic speeds, pressure drag on the longer of two boattail configurations was equal to or less than the pressure drag on the shorter configuration. At subsonic and transonic speeds, the difference in C_D was on the order of 0.0008 to 0.0010. In the supersonic cruise range, the difference in C_D was on the order of 0.0002. Boattail drag coefficients are based on wing reference area.

INTRODUCTION

The economic feasibility of long range supersonic cruise airplanes, including current supersonic transports, is clearly dependent on design efficiency. Even slight increases in drag can cause large fuel penalties and substantially increase the overall operating costs of the airplane. Since the development of "second generation" supersonic transports is dependent on their ability to compete economically with current wide-bodied jets, designers of these airplanes must have both sufficient data and suitable analytical tools to accurately predict aerodynamic characteristics at supersonic cruise conditions. Unfortunately, in some cases, these needs are not adequately met.

For example, approximately one-third of the cruise drag of a typical supersonic transport airplane is attributed to skin friction; therefore, any prediction of flight performance must include an accurate accounting of full-scale, high Reynolds number, viscous flow characteristics. Since full-scale flow characteristics can differ significantly from those measured on small-scale models in a wind tunnel environment, correlation between the two is obtained by adjustments which primarily account for the Reynolds number differences. These adjustments are usually based on empirical data obtained for two-dimensional flow over smooth flat plates or on measurements taken along wind tunnel walls. However, recent studies indicate that these methods may not necessarily provide the accurate full-scale skin friction predictions that are essential for the development of efficient airplane designs.

Similar limitations are also found in fuselage closure or afterbody design. In this case, both predictive techniques and quantitative experimental data are lacking for the high Reynolds number, thick boundary layer conditions encountered in supersonic cruise flight, particularly when the possibility of afterbody flow separation exists. In wind tunnel tests, afterbody drag is usually estimated rather than measured because of the cost and complexity of the model, support structure, and data acquisition system needed to obtain accurate afterbody measurements. However, even when such needs are met, it is obvious that very thick boundary layer data cannot be obtained using models and existing supersonic wind tunnel facilities.

Although some data have been previously obtained in flight (refs. 1 to 3), suitable data are still lacking. Because of this, and because of limitations in present high Mach number predictive techniques, NASA initiated the flight experiments program using the YF-12A and YF-12C airplanes. As part of these experiments, skin friction and boundary layer data, as well as boattail pressures, were obtained for Reynolds numbers up to 4×10^8 and speeds up to Mach 3.0. Skin friction coefficients and boundary layer characteristics were measured on the lower fuselage centerline of the YF-12A airplane. Boattail pressures from two YF-12 afterbody configurations were obtained and analyzed to determine differences in pressure drag between the two configurations for both subsonic and supersonic flight conditions.

SYMBOLS

Physical quantities in this report are given in the International System of

Units (SI). Measurements were taken in U.S. Customary Units.

C_D	drag coefficient
C_f	local skin friction coefficient
C_p	pressure coefficient, $\frac{p - p_\infty}{q_\infty}$
L	fuselage length, m
M	Mach number
M_∞	free stream Mach number
p	local static pressure, N/m^2
p_∞	free stream static pressure, N/m^2
q_∞	free stream dynamic pressure, N/m^2
R_x	Reynolds number based on distance, x
R_θ	Reynolds number based on momentum thickness
T_1	static temperature at edge of boundary layer, K
T'	reference temperature (ref. 9), K
u/u_1	ratio of local velocity to boundary layer edge velocity
x	distance from nose apex, m
y	distance from surface to rake probe centerline, cm
α	wing angle of attack, deg
δ	boundary layer thickness, $u/u_1 = 0.99$, cm
δ^*	displacement thickness of boundary layer, cm
θ	momentum thickness of boundary layer, cm
μ_1	absolute viscosity based on edge temperature
μ'	absolute viscosity based on reference temperature

TEST DESCRIPTION

Boundary Layer Skin Friction Experiment

Measurements were taken at five boundary layer, skin friction stations on the lower fuselage of the YF-12A airplane. The stations were located 3.9, 7.3, 12.1, 18.6, and 24.1 meters aft of the nose apex to provide a history of the boundary layer flow along the lower fuselage surface. Tests were conducted with only one station mounted at a time. That station was instrumented with a boundary layer rake, a static pressure orifice, one to four Preston probes, and a skin surface thermocouple. A skin friction balance was also used at the two forward stations.

In order to provide an undisturbed flow over the lower fuselage, all upstream protrusions, bleeds, and vents were removed. This was accomplished by placing fairings over the nose vent and nose gear compartment vents and by rerouting the cooling air from the compartments out of an aft-facing vent on the upper surface of the left chine. In addition, a cooling air scoop on the right hand missile bay door was removed.

Boattail Drag Experiment

In flight, surface static pressures were measured on two boattail configurations of the YF-12 aircraft. Figure 3 provides a general view of the airplane showing the two boattail configurations and the radial locations of the static pressure orifices used on the YF-12A airplane. The YF-12C airplane does not have a lower centerline-mounted ventral fin; therefore, an additional row of static pressure orifices was installed along the lower fuselage centerline.

The YF-12A boattail had a fineness ratio of 4.6. The YF-12C boattail was 1.14 meters longer than the YF-12A configuration and had a fineness ratio of 5.3. Figure 4 provides detailed views of both configurations and indicates the fuselage stations at which the boattail begins on each of the two airplanes.

TEST CONDITIONS

The skin friction data were obtained at Mach numbers between 2.0 and 3.0 and at Reynolds numbers up to 2×10^8, based on the run length. Boundary layer rake data were obtained at three nominal Mach numbers: 2.0, 2.5, and 3.0. Boattail pressures were measured from subsonic Mach numbers up to Mach 3.0 and at Reynolds numbers up to 4×10^8, based on fuselage length. All data were obtained in stabilized level flight using a modified autopilot altitude hold mode which is described in reference 4. The use of the altitude hold mode enabled altitude to be held constant, thus minimizing lag effects.

The angle-of-attack range for the boundary layer skin friction experiment varied from 2.8° to 5.5°. For the boattail experiment, the angle of attack varied from 1.0° to 5.5° on the YF-12A airplane and from 2.0° to 5.5° on the YF-12C airplane.

INSTRUMENTATION

The two primary air data reference parameters, free stream Mach number, M_∞, and free stream static pressure, p_∞, were measured using identical pitot static probes (fig. 5) mounted on the nose boom on each aircraft. Descriptions of the probe and its flight calibration are presented in reference 5. Free stream total temperature was measured with a thermocouple-type total temperature probe mounted on the upper surface of the nose.

Pressures obtained from boundary layer rakes, Preston probes, and static pressure orifices were measured using several differential pressure transducers and scanning mechanisms. Transducer ranges were selected to optimize measurement accuracies, and each transducer was referenced to a closely monitored precise reference pressure. The skin friction force balance used in these tests was the same type as described in reference 6. All data were acquired by a nine bit pulse code modulated data system and recorded, in digital form, on magnetic tape.

RESULTS AND DISCUSSION

Boundary Layer Skin Friction Experiment

Velocity profiles for the five lower fuselage locations are presented in figure 6 for nominal Mach numbers of 2.0, 2.5, and 3.0 In general, the profiles have a logarithmic shape except for some distortion at station 2 and, to a lesser extent, at station 3. The distortion becomes most pronounced at Mach 3.

Figure 7 shows the growth of the boundary layer, δ, displacement thickness, δ^*, and momentum thickness, θ, as a function of fuselage length for each of the test Mach numbers. Figure 7(c) includes theoretical estimates of the displacement and momentum thickness computed using the finite difference method described in reference 7. At Mach 3.0 the theoretical predictions agree with the mean values of the flight measurements at stations 1 and 5; however, at stations 2, 3, and 4 the measured values of displacement and momentum thickness are much larger than predicted. For example, at station 2 the measured value exceeds the predicted value by a factor of about 2.8. The fact that thickness parameters may be significantly larger than predicted suggests that extra care must be taken in designing and locating engine inlets and cooling air intakes for supersonic cruise applications in order to prevent the ingestion of low energy boundary layer air.

At stations 1 and 2, local skin friction coefficients were measured using skin friction force balances and Preston probes. The Preston probes were calibrated using the technique described in reference 8. In figure 8 the friction coefficient values obtained using the Preston probes are plotted as a function of the corresponding values obtained using the friction force balance. The line of perfect agreement represents the locus of points for which the two techniques yield identical results. The root-mean-square value of the scatter about the line of perfect agreement for the Preston probe at station 1 was ± 2 percent. At station 2, the Preston probe results were biased about 5 percent high, and, the root-mean-square error was on the

order of ±4 percent. The good agreement between the values confirms the findings of reference 1 which indicate that the Preston probes can provide reliable skin friction coefficients in the supersonic cruise environment. This is significant since the Preston probes are less expensive, easier to install and maintain, and less susceptible to damage. Also, unlike the force balance units, they do not require cooling at the higher Mach numbers, and they can be installed in locations where there is insufficient space beneath the skin to install a friction force balance.

In figure 9(a), the local friction coefficients obtained using the friction force balance at stations 1 and 2 are plotted as a function of Reynolds number based on run length, R_x. In figure 9(b), the same values are plotted as a function of Reynolds number based on momentum thickness, R_θ. In these plots the friction coefficients and Reynolds numbers have been normalized to a Mach number of 0 using the Sommer and Short *T-prime* method described in reference 9.

The local friction coefficients from station 1 agree reasonably well with the von Kármán-Schoenherr flat plate theory; however, for station 2, the skin friction coefficients plotted as a function of R_x are about 30 percent lower than predicted and those plotted as a function of R_θ are about 20 percent lower than predicted.

In figures 10(a) and 10(b), friction coefficients obtained by the Preston probe technique are plotted as functions of R_x and R_θ for all five stations. Most of the skin friction coefficients for stations 1, 4, and 5 fall near the von Kármán-Schoenherr theoretical values, tending to be slightly lower at the highest Reynolds numbers; however, the data from stations 2 and 3 are significantly lower than predicted. The differences at station 2 amount to about 30 percent for the R_x plot and about 20 percent for the R_θ plot. At station 3 the coefficients in the same two plots were about 35 to 25 percent lower, respectively. However, even though the skin friction at stations 2 and 3 was lower than predicted, it should not be concluded that the overall skin friction drag was lower. A limited number of skin friction measurements made on the upper centerline of the YF-12A airplane (ref. 10) indicate that local skin friction coefficients at those stations were 17 to 23 percent higher than predicted by flat plate theory. Similarly, local skin friction coefficients measured on the upper fuselage centerline of the XB-70 airplane (ref. 1) were approximately 25 percent higher than predicted for a Mach number range of 2.0 to 2.5. These findings suggest that flat plate theory extrapolations from low Reynolds number model measurements to high Reynolds number flight predictions are sometimes dependent upon compensating differences in skin friction effects over the various parts of the aircraft.

Because of the unusual boundary layer profiles and low skin friction coefficients obtained at station 2, additional tests and analyses were performed in an attempt to find an explanation for the anomolies observed in the data. It was first hypothesized that a strong adverse pressure gradient might have existed very near station 2. To investigate this possibility, pressure coefficient data from previously unpublished one-twelfth-scale model wind tunnel tests and in-flight data obtained from several local flush orifices were examined. Figure 11 presents the pressure coefficients measured along the lower fuselage centerline of the one-twelfth-scale model along with the in-flight measurements. Neither the wind tunnel nor the flight data provide

any indication that a strong adverse longitudinal pressure gradient exists at station 2.

Other possible causes could have been the presence of a pressure gradient through the boundary layer or the presence of crossflow conditions near station 2. To investigate these possibilities, additional instrumentation was added to the airplane; however, subsequent tests detected only very slight gradients and crossflow conditions which were insufficient to cause the anomolies at station 2.

While the unexpected shape of the boundary layer and the increased thickness parameters cannot be explained at present, they represent real and repeatable flow conditions over a three-dimensional shape with practical surface construction, lifting surfaces, and three-dimensional flow.

Boattail Drag Experiment

Figure 12 provides boattail pressure coefficients for both the YF-12A and YF-12C configurations for several representative Mach numbers. At a Mach number of 0.7 (fig. 12(a)), the upper surface pressure coefficients for the YF-12C configuration are significantly more positive than those for the YF-12A configuration at normalized fuselage locations, x/L, of 0.80 to 0.93. Similar characteristics can be noted along the lower surface for values of x/L from 0.90 to 0.98. The more positive pressures indicate that the YF-12C boattail configuration offers less subsonic pressure drag at a Mach number of 0.7.

In figure 12(b), a similar comparison of boattail pressure coefficients at Mach 0.96 shows significantly more positive values for nearly the entire upper boattail region of the YF-12C configuration as well as for x/L values from 0.90 to 0.98 on the lower surface.

Fewer apparent differences are present at a Mach number of 1.12 (fig. 12(c)) except for a local region between x/L locations of about 0.80 to 0.85 on the upper surfaces and at x/L locations greater than 0.93 on the lower surfaces. The pressure coefficients for the YF-12C configuration become positive aft of about an x/L location of 0.97 on both the upper and lower surfaces. A fuel dump nozzle on the YF-12A airplane prevented the installation of static pressure orifices on the aft-most portion of the boattail; therefore, it is uncertain if positive pressure coefficients were present at these locations on the YF-12A configuration. It is suspected that the additional 1.14 meters length of the YF-12C boattail may extend through a region of influence from the engine exhaust flow field. Further flight tests are planned to determine if engine power settings influence the YF-12C boattail pressures.

Pressure distributions for Mach numbers of 2.0 and 3.0 are presented in figures 12(d) and 12(e), respectively. Although the YF-12C airplane has higher upper surface pressure coefficients in these speed ranges, there are compensating effects in favor of the YF-12A configuration over parts of the lower boattail surfaces. When the pressure coefficients are integrated to determine the overall boattail pressure drag for the two configurations, it is found that the YF-12C configuration has a slight advantage at Mach 2.0. However, this slight advantage becomes significant if the vehicle must cruise at this speed for extended periods of time.

A version of the Woodward-Carmichael computer program (ref. 11) was used to estimate the potential pressure distribution of the YF-12 wing planform. The afterbodies were modeled as wing thicknesses. The program provides a reasonably accurate analytical estimate of the pressure distribution under potential, attached, and inviscid flow conditions at both subsonic and supersonic Mach numbers. The presence of large differences between analytical results and flight measurements affords a method for identifying nonpotential flow such as can exist when vortex interactions, separated flow conditions, large viscous effects, or transonic flow anomalies are present. It has been postulated that at low speeds the upper surfaces of the YF-12 airplanes are affected by vortex flow. This postulate is supported by the large differences between the analytical results and the flight measurements shown in figure 13(a). However, such an interpretation is inappropriate for the supersonic data shown in figures 13(b) and 13(c) where the differences are too small to be conclusive.

Figure 14 shows the overall boattail pressure drag results obtained for the entire Mach number range studied. Pressure coefficients for both configurations have been integrated over the respective projected areas of the aft-sloping surfaces, and the wing reference area has been used to compute the boattail drag coefficients. This plot shows that the longer boattail configuration on the YF-12C airplane has significantly less boattail pressure drag up to a Mach number of 1.2, and slightly less boattail pressure drag from Mach 2.0 to Mach 2.5. The longer length and higher fineness ratio of the YF-12C configuration caused the boattail pressure drag coefficient to peak at Mach 1.2 instead of at Mach 1.05 as for the YF-12A configuration. Subsonically, the pressure drag coefficients for the YF-12C configuration are 8 to 10 counts (1 count = 0.0001 C_D) less than those for the YF-12A configuration. At Mach 1.05 the reduction in the pressure drag coefficients is on the order of 9.5 counts, and in the Mach number range from 2.0 to 2.5, the YF-12C boattail pressure coefficients are about 2 counts less.

It should be noted that the apparent advantage in boattail pressure drag due to the higher fineness ratio on the YF-12C airplane may not provide the same increment of drag improvement when applied to a specific airplane. A longer boattail can be expected to result in increased friction, weight, and volume, and it could result in more or less trim drag, depending on the specific aircraft configuration. However, assuming the same values of thrust, weight, volume, and trim drag, the reduced pressure drag could offer a significant advantage in transonic acceleration. On the YF-12C airplane the improvement amounts to about 0.01g or an equivalent thrust increase of about 2 percent.

While these pressure drag differences may seem insignificant on the YF-12 airplanes because of their large excess thrust, they could become significant on a supersonic transport aircraft operated in a competitive commercial environment. For a 200 to 250 passenger supersonic transport aircraft, fuel savings could amount to about 900 kilograms per hour at subsonic loiter, about 1100 kilograms per hour at subsonic cruise, and about 600 kilograms per hour at a supersonic cruise Mach number of 2.3.

CONCLUDING REMARKS

Boundary layer, skin friction, and boattail pressure distribution data have been obtained in flight using the YF-12 airplanes. The boundary layer data were obtained for Mach numbers between 2.0 and 3.0 and the boattail pressure data were measured from Mach 0.7 to Mach 3.0 at Reynolds numbers up to 4×10^8.

Boundary layer data measured along the lower fuselage centerline of the YF-12A airplane indicate that local displacement and momentum thickness parameters can be much larger than predicted. The possibility of larger momentum thicknesses should be a consideration in the design and integration of engine inlets and cooling air scoops for supersonic cruise vehicles.

It was determined that local skin friction coefficients at two of five lower fuselage centerline stations were significantly less than predicted by flat plate theory. However, flight results from other experiments have shown local friction coefficients on upper surface locations to be higher than predicted (refs. 1 and 10). Such compensating effects may be a forgiving factor when model to full-scale flight friction drag adjustments are made using the usual flat plate, two-dimensional Reynolds number and drag relationships.

Large differences between measured boattail pressures and values calculated by the Woodward-Carmichael potential flow solution suggest the presence of vortex flow effects on the upper surfaces of the YF-12 boattail at subsonic speeds.

At subsonic speeds the pressure drag coefficients of the longer boattail configuration of the YF-12C were 8 to 10 counts less than the coefficients for the shorter YF-12A configuration. At Mach numbers from 2.0 to 2.5, pressure drag coefficients of the longer configuration were approximately 2 counts less. These same values, if projected for a supersonic transport aircraft of about 200 to 250 passenger capacity, could result in a fuel savings of about 900 kilograms per hour at subsonic loiter, about 1100 kilograms per hour at subsonic cruise, and about 600 kilograms per hour at a supersonic cruise Mach number of 2.3.

REFERENCES

1. Fisher, David F.; and Saltzman, Edwin J.: Local Skin Friction Coefficients and Boundary-Layer Profiles Obtained in Flight From the XB-70-1 Airplane at Mach Numbers up to 2.5. NASA TN D-7220, 1973.

2. Saltzman, Edwin J.; and Fisher, David F.: Some Turbulent Boundary-Layer Measurements Obtained From the Forebody of an Airplane at Mach Numbers up to 1.72. NASA TN D-5838, 1970.

3. Erlich, E.: Sondage de la Couche Limite en Vol Supersonique sur L'Avion "Mirage IV." O.N.E.R.A. Paper Presented at 3^{e} Colloque Aerodynamique de l'A. F.I.T.A.E., Marseille, France, Nov. 8-10, 1966.

4. Gilyard, Glenn B.; and Smith, John W.: Flight Experience With Altitude Hold and Mach Hold Autopilots on the YF-12 Aircraft at Mach 3. Proceedings of YF-12 Experiments Symposium, NASA CP-2054, Vol. 1, 1978.

5. Larson, Terry J.: Compensated and Uncompensated Nose Boom Static Pressures Measured From Two Air Data Systems on a Supersonic Airplane. NASA TM X-3132, 1974.

6. Garringer, Darwin J.; and Saltzman, Edwin J.: Flight Demonstration of a Skin-Friction Gage to a Local Mach Number of 4.9. NASA TN D-3830, 1967.

7. Albers, James A.; and Gregg, John L.: Computer Program for Calculating Laminar, Transitional, and Turbulent Boundary Layers for a Compressible Axisymmetric Flow. NASA TN D-7521, 1974.

8. Hopkins, Edward J.; and Keener, Earl R.: Study of Surface Pitots for Measuring Turbulent Skin Friction at Supersonic Mach Numbers — Adiabatic Wall. NASA TN D-3478, 1966.

9. Sommer, Simon C.; and Short, Barbara J.: Free-Flight Measurements of Turbulent-Boundary-Layer Skin Friction in the Presence of Severe Aerodynamic Heating at Mach Numbers From 2.8 to 7.0. NACA TN-3391, 1955.

10. Powers, Sheryll Goecke: Flight-Measured Pressure Characteristics of Aft-Facing Steps in High Reynolds Number Flow at Mach Numbers of 2.20, 2.50, and 2.80 and Comparison With Other Data. NASA TM-72855, 1978.

11. Woodward, Frank A.: Analysis and Design or Wing-Body Combinations at Subsonic and Supersonic Speeds. J. Aircraft, vol. 5, no. 6, Dec. 1968, pp. 528-534.

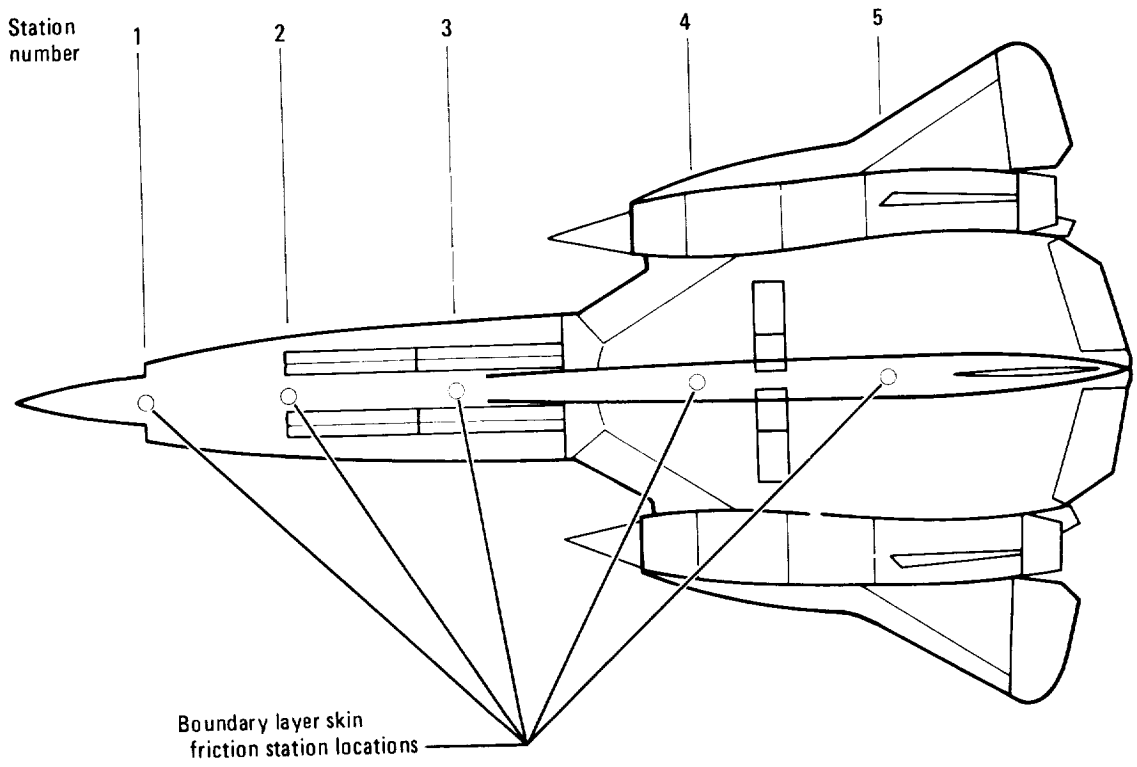

Figure 1.—Bottom view of YF-12A airplane showing locations of boundary layer skin friction stations.

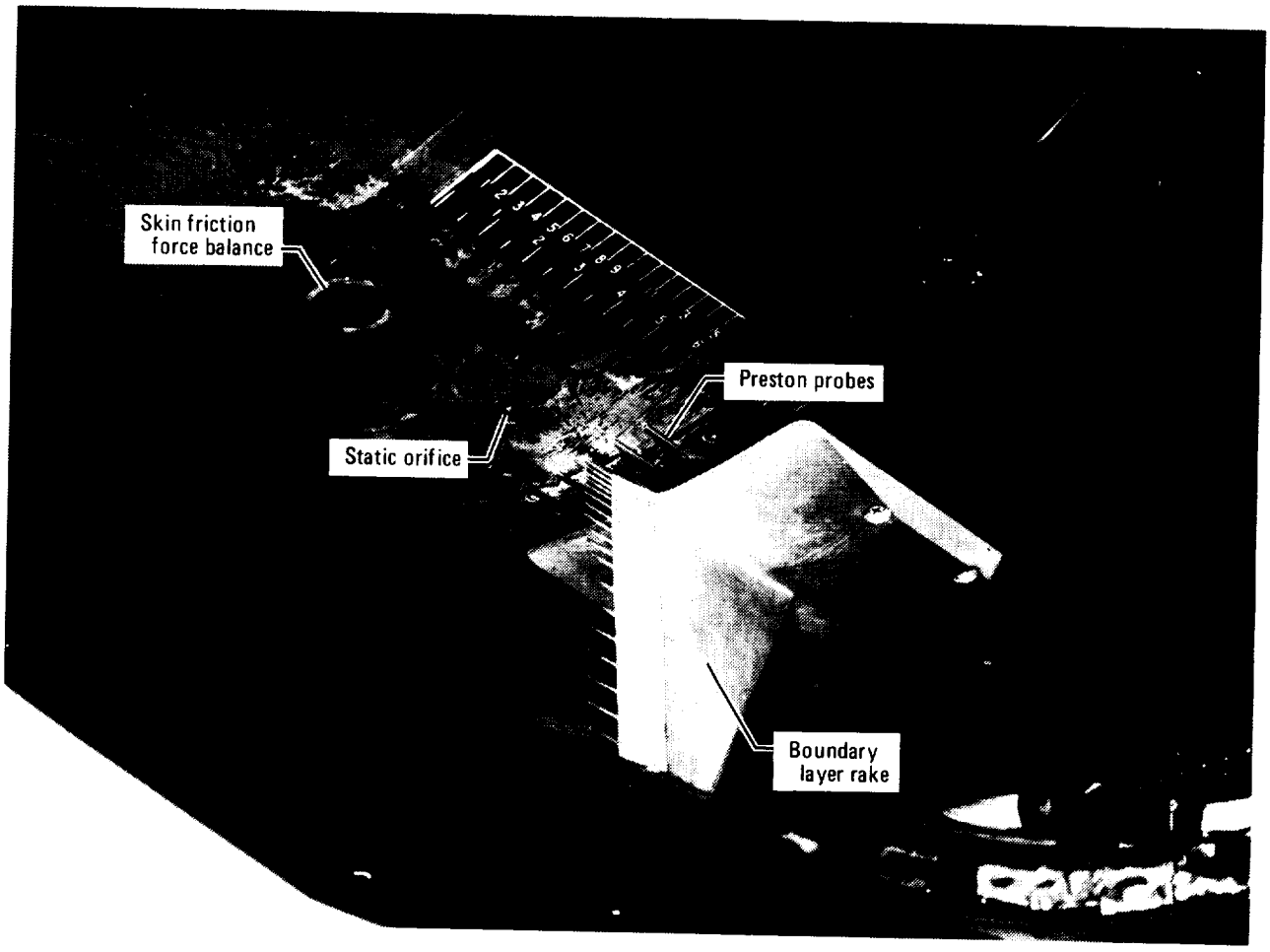

Figure 2.—Photo of typical boundary layer skin friction station showing the boundary layer rake, Preston probes, skin friction force balance, and static orifice.

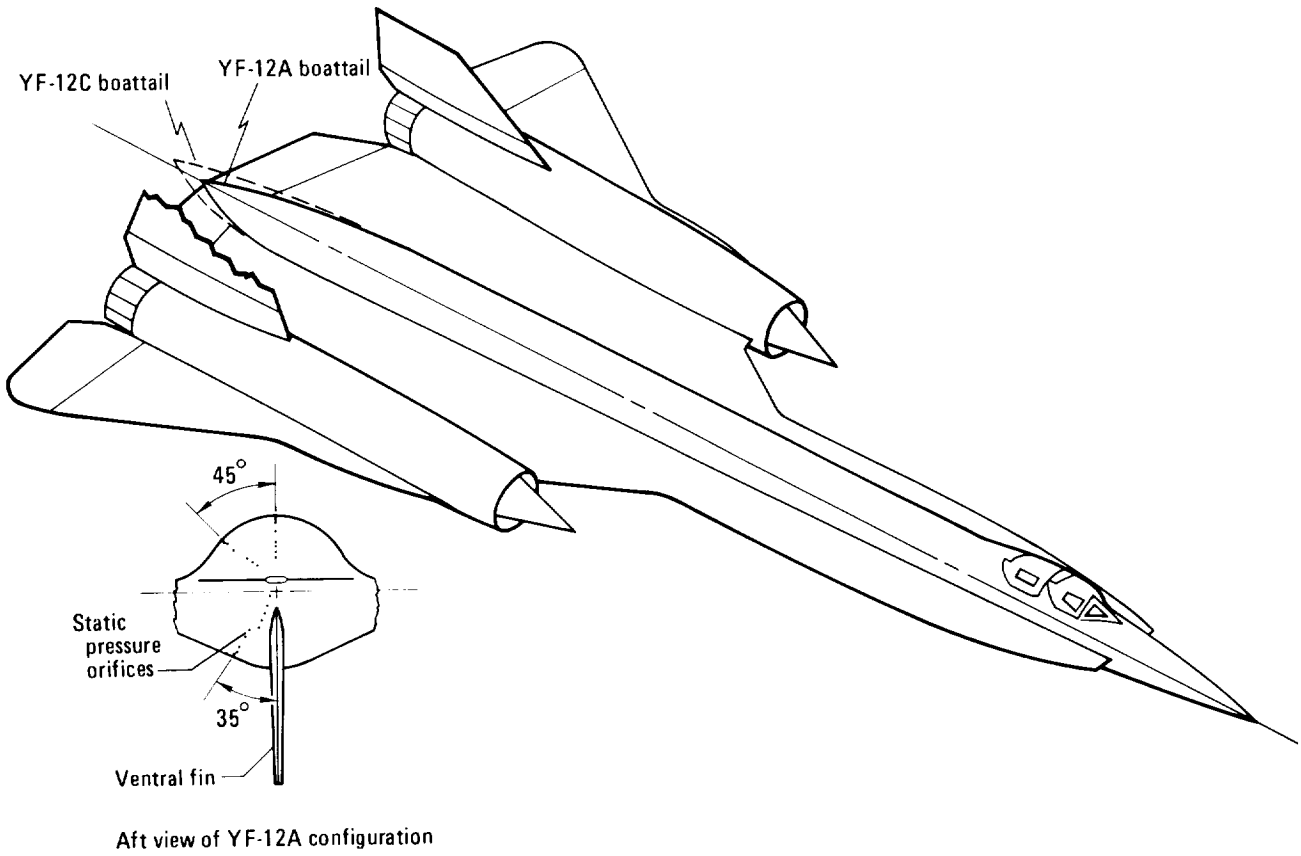

Figure 3.—General view of YF-12 airplane showing the two boattail configurations and radial location of static pressure orifices on configuration A.

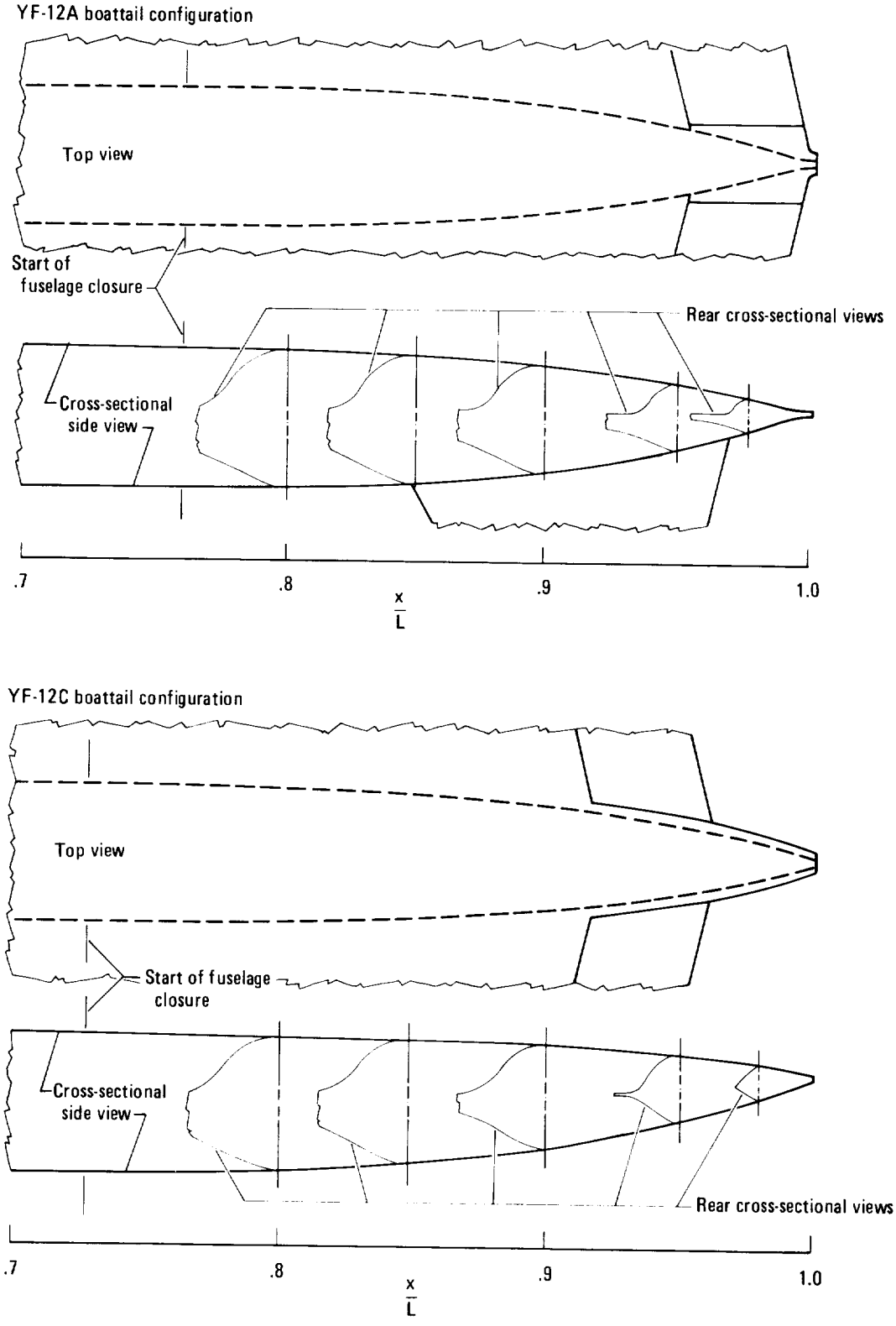

Figure 4.—Views of YF-12 boattails, configurations A and C.

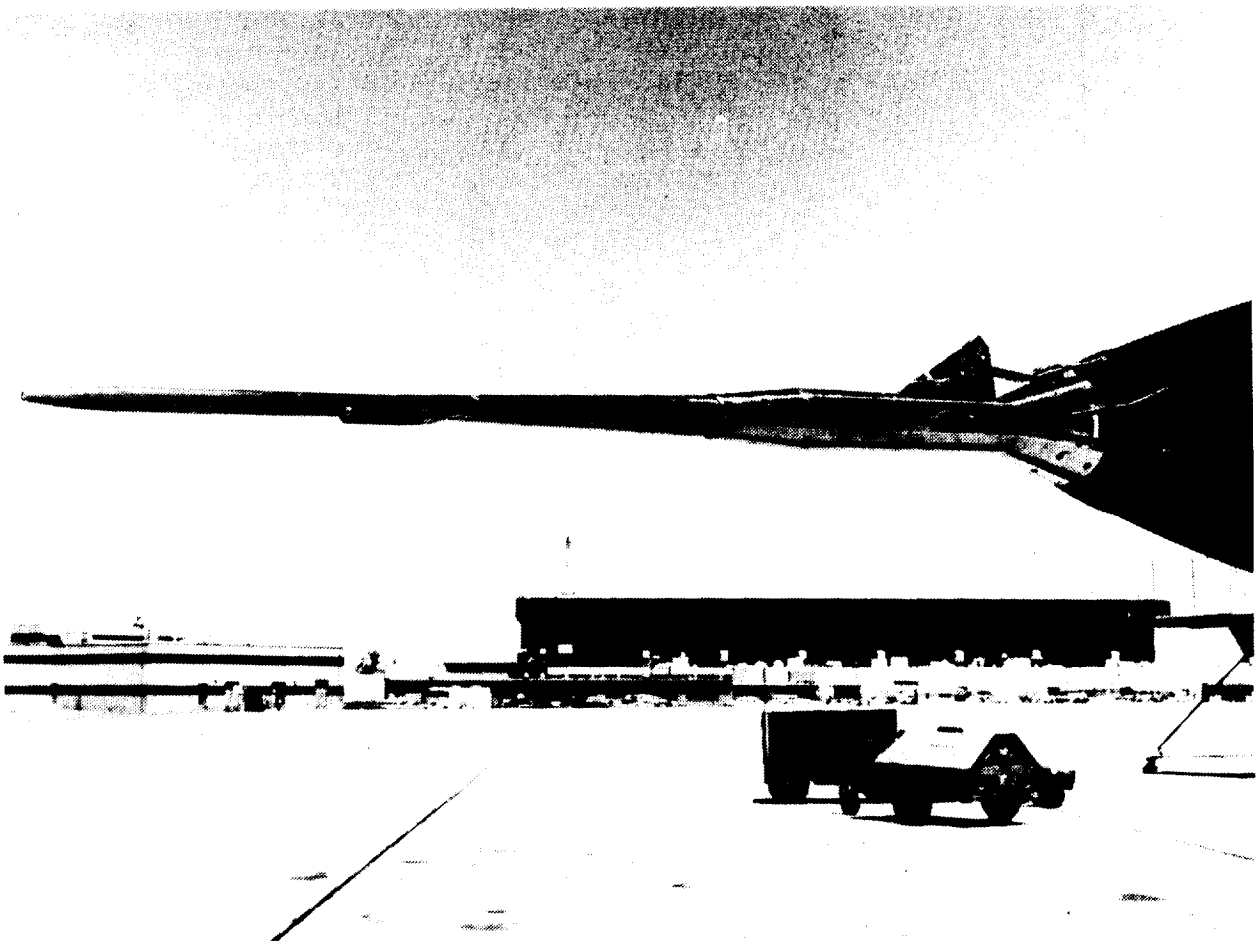

Figure 5.—Photo of airspeed probe.

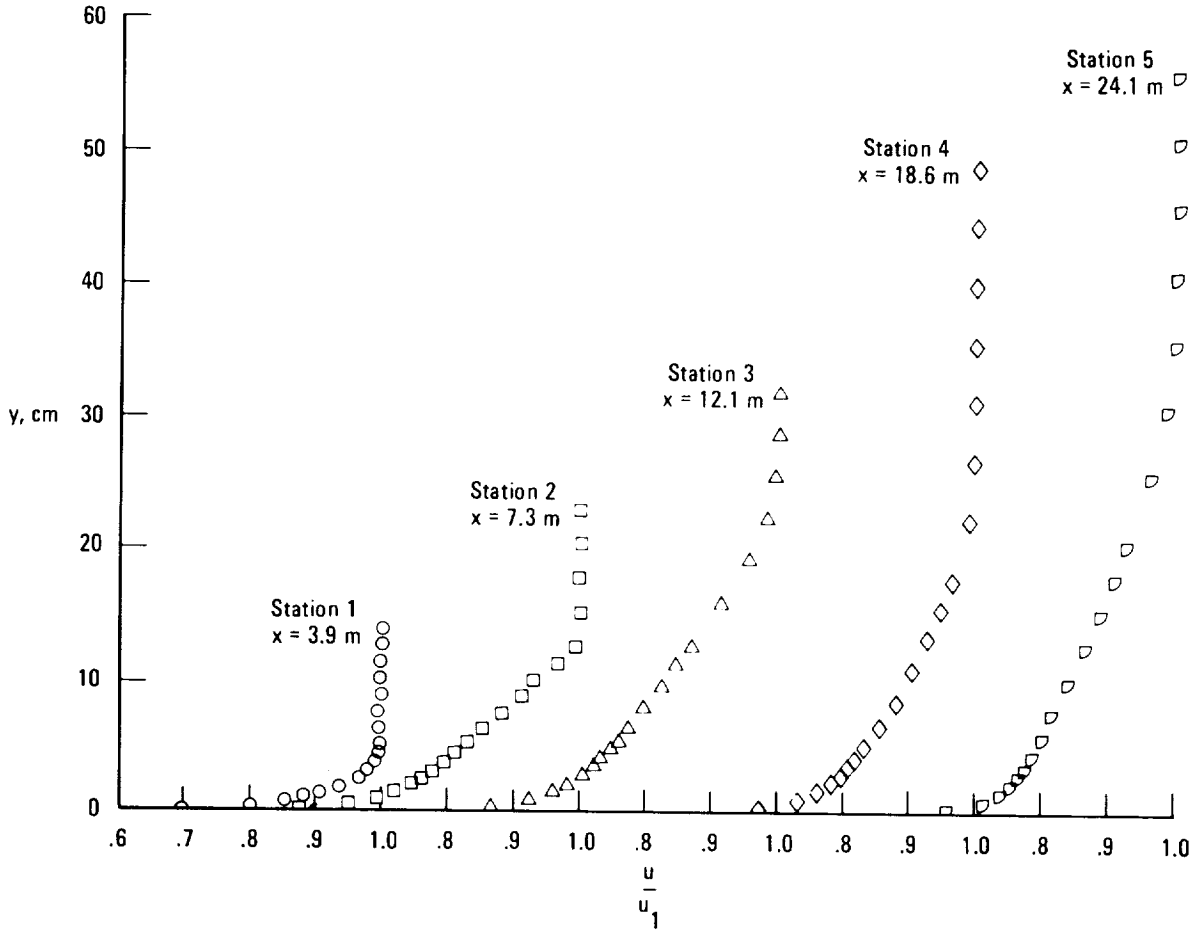

(a) $M \approx 2.0$.

Figure 6.—Boundary layer velocity profiles from five stations along the lower fuselage centerline of the YF-12A.

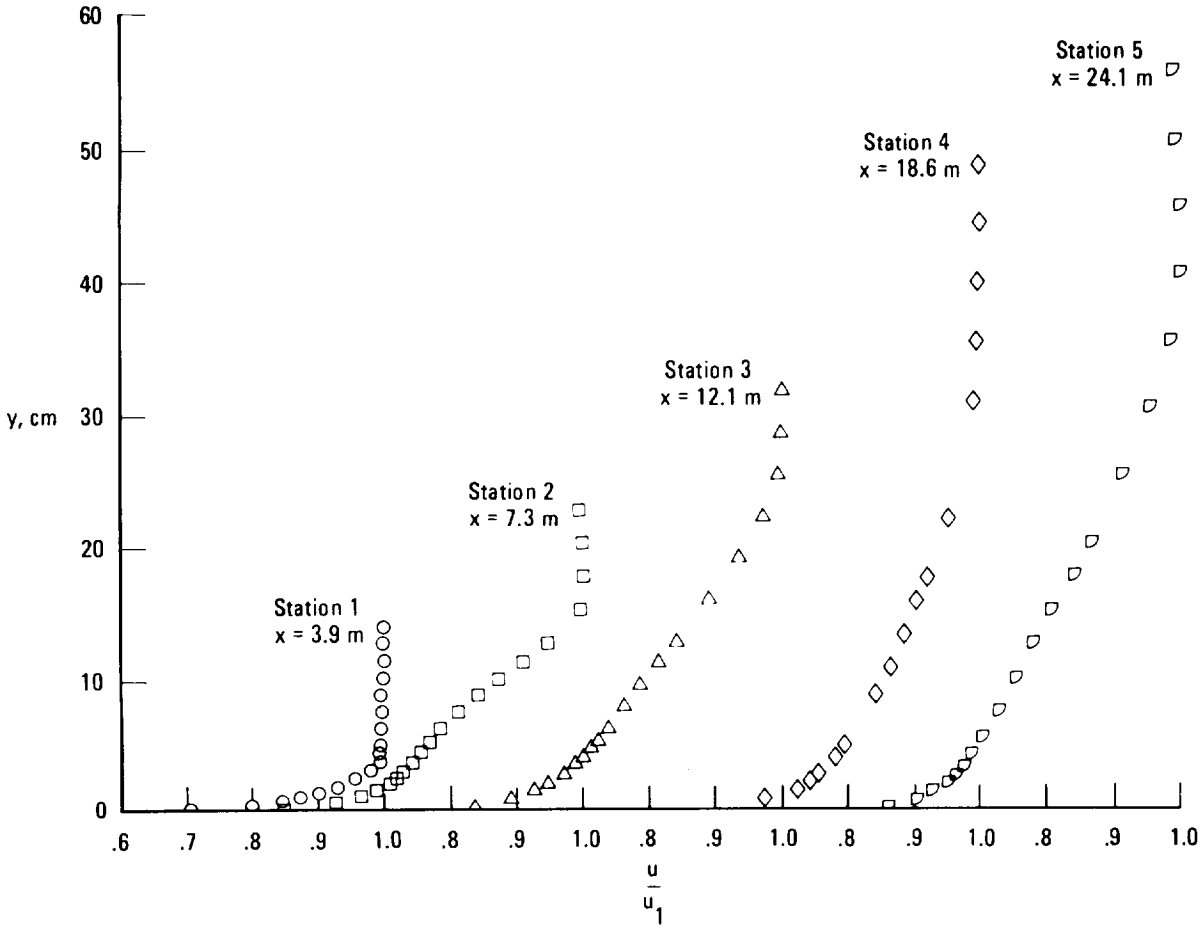

(b) $M \approx 2.5$.

Figure 6.—Continued.

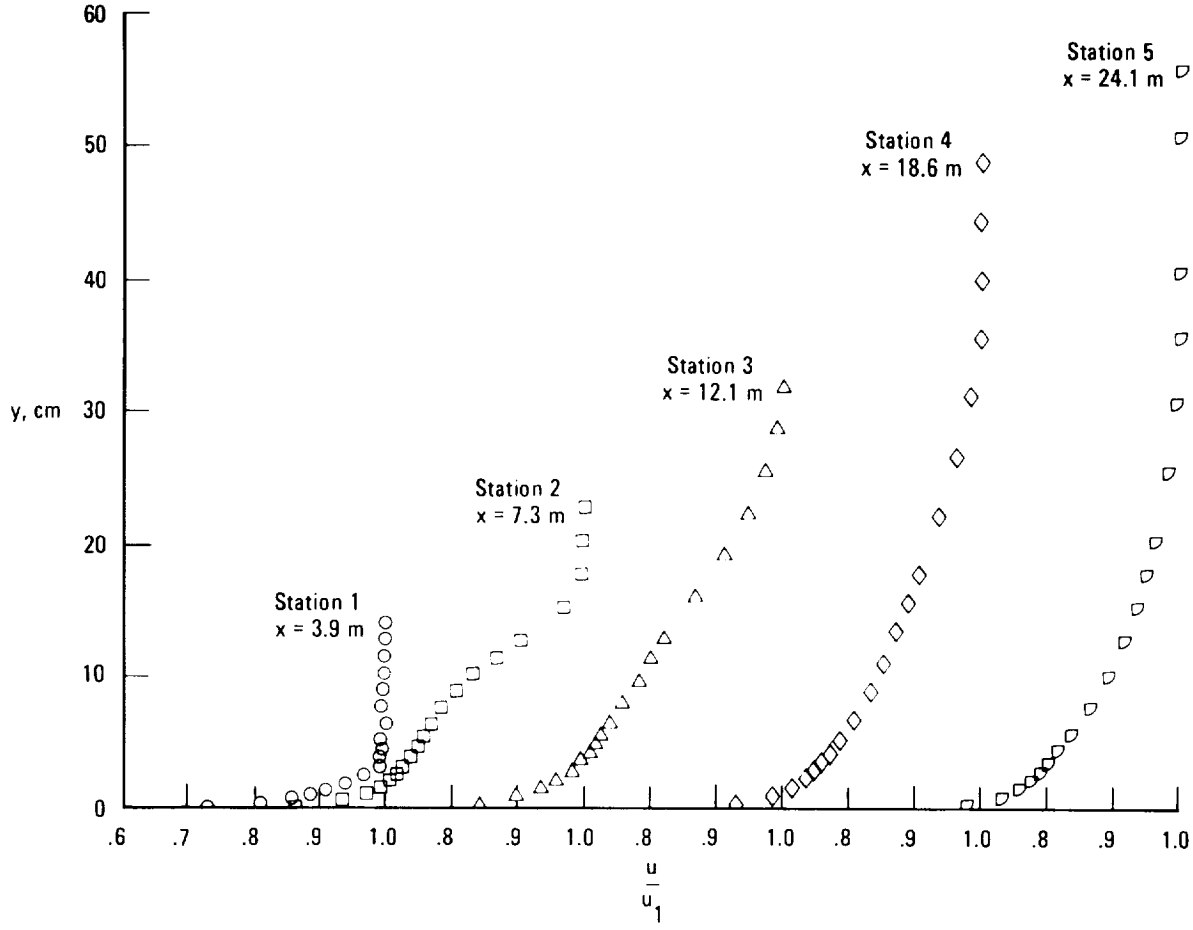

(c) $M \approx 3.0$.

Figure 6.—Concluded.

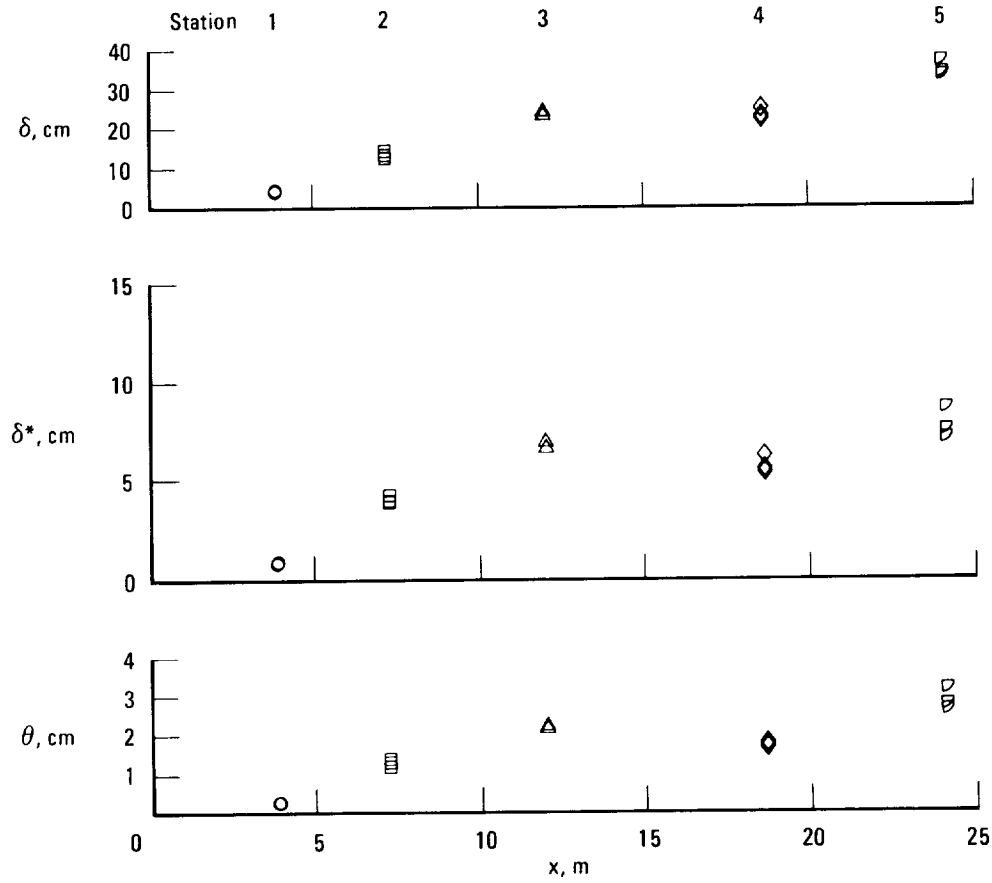

(a) $M \approx 2.0$.

Figure 7.—Variation of boundary layer thickness, δ, displacement thickness, δ*, and momentum thickness, θ, as a function of run length, x.

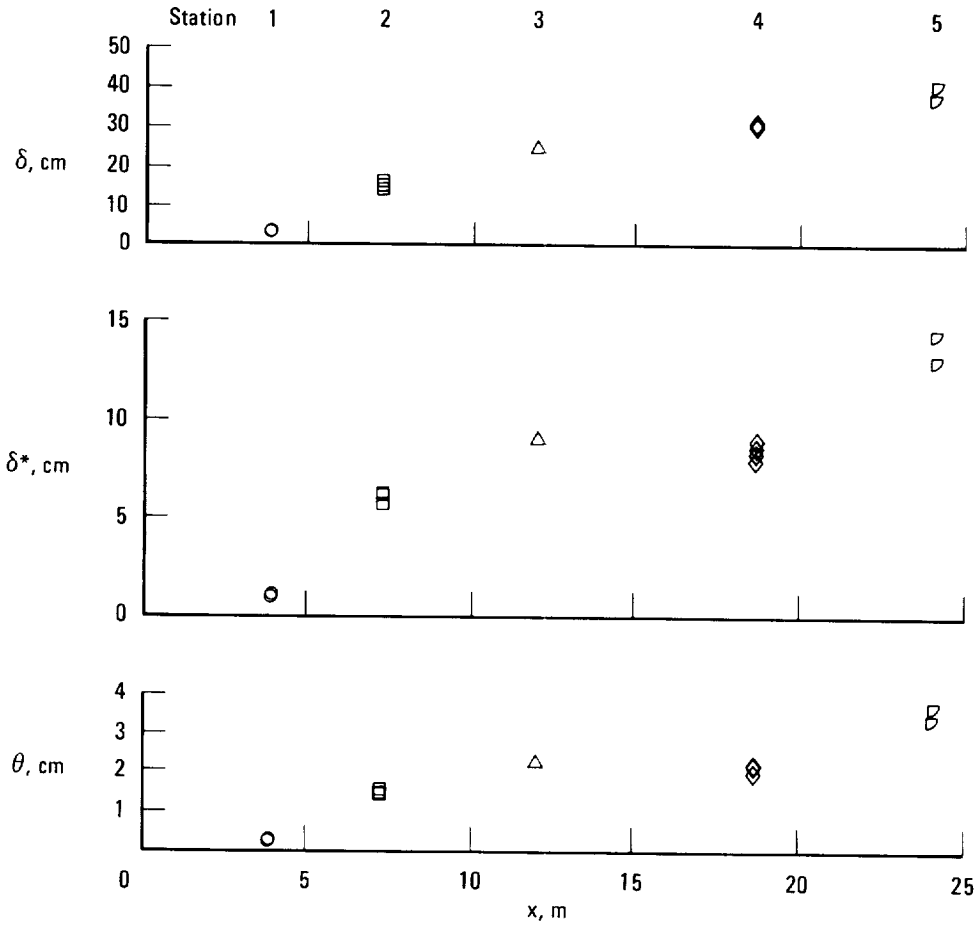

(b) $M \approx 2.5$.

Figure 7.—Continued.

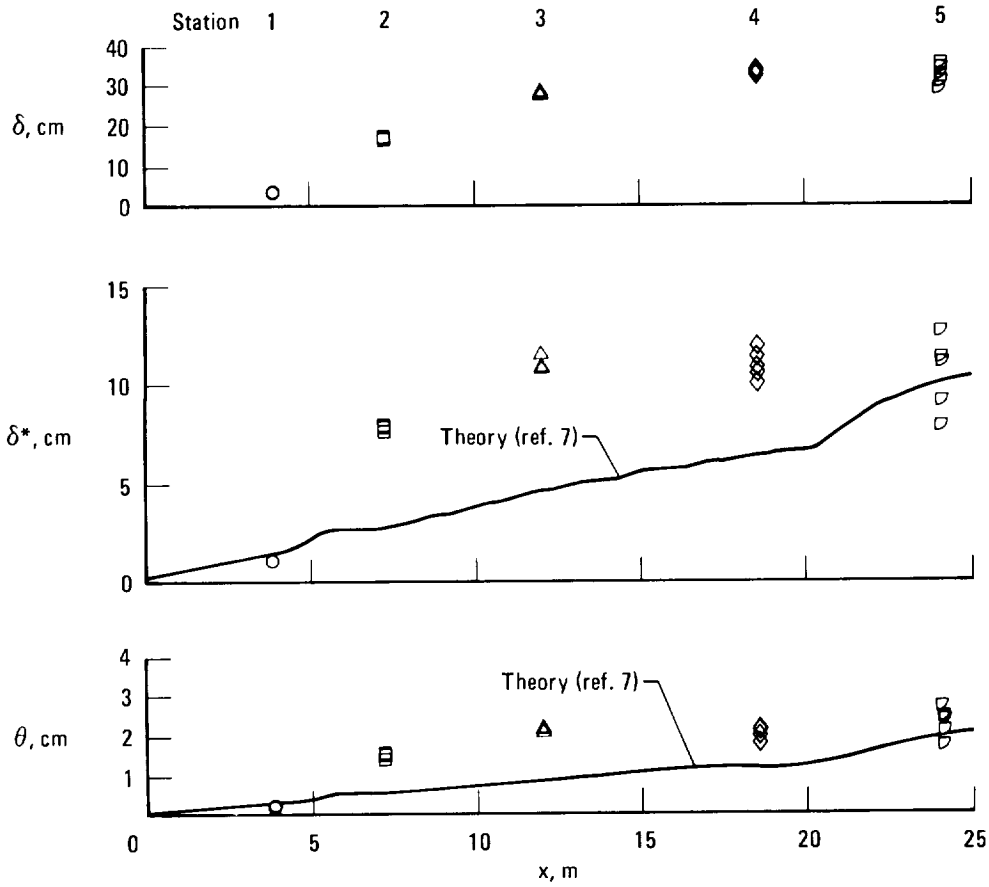

(c) $M \approx 3.0$.

Figure 7.—Concluded.

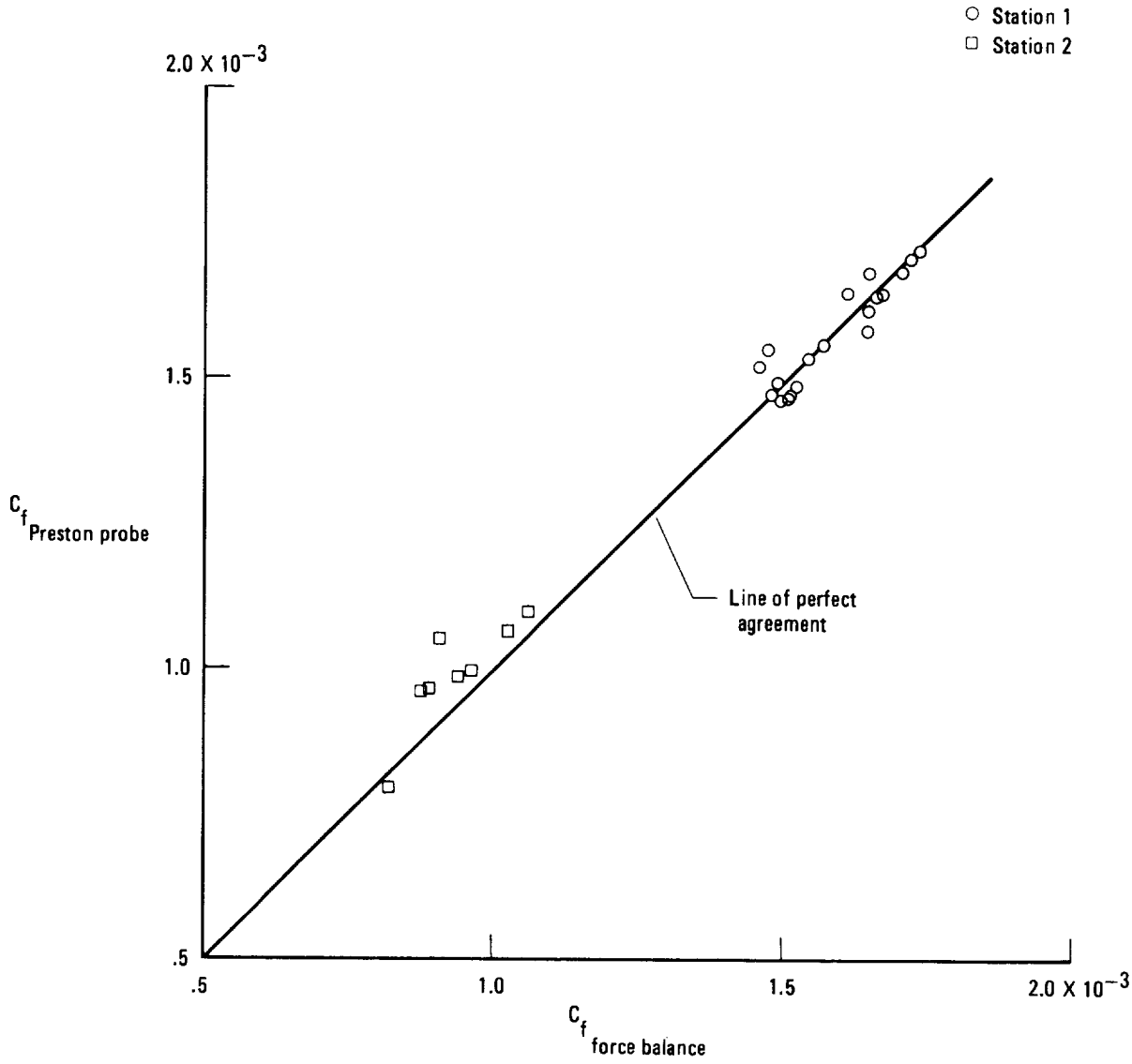

Figure 8.—Comparison of Preston probe skin friction coefficients determined by the Hopkins-Keener calibration with the skin friction coefficients obtained by the force balance technique.

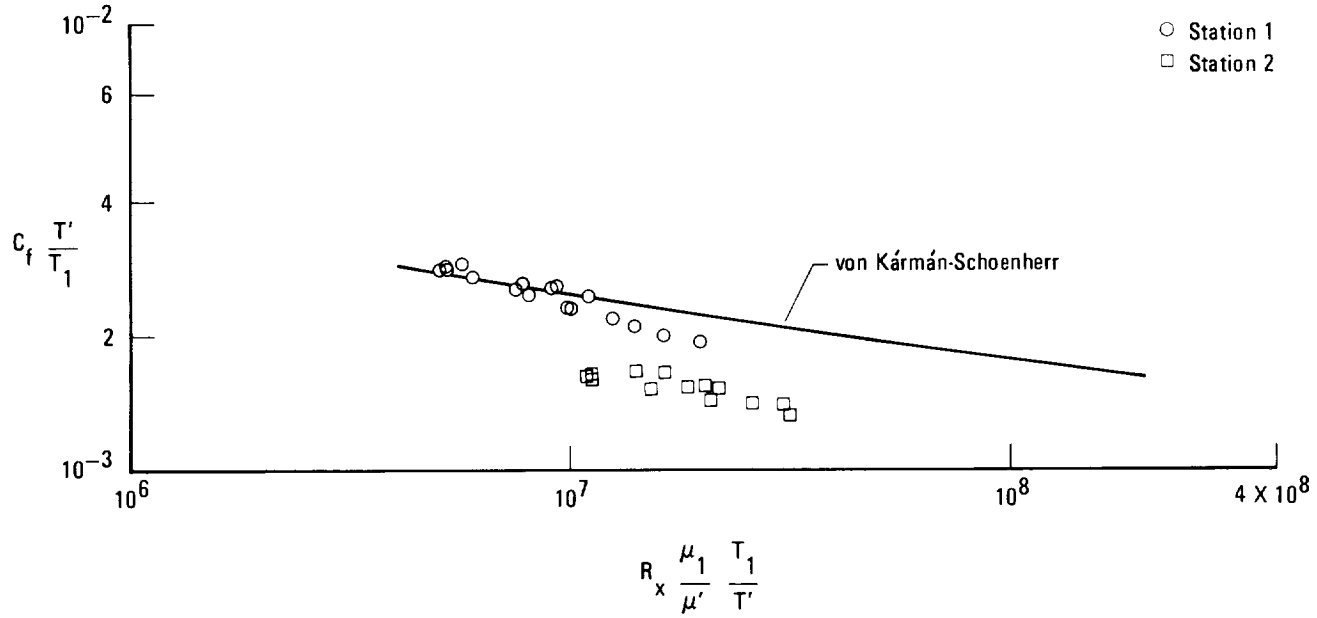

(a) Reynolds number based on x, distance from nose apex.

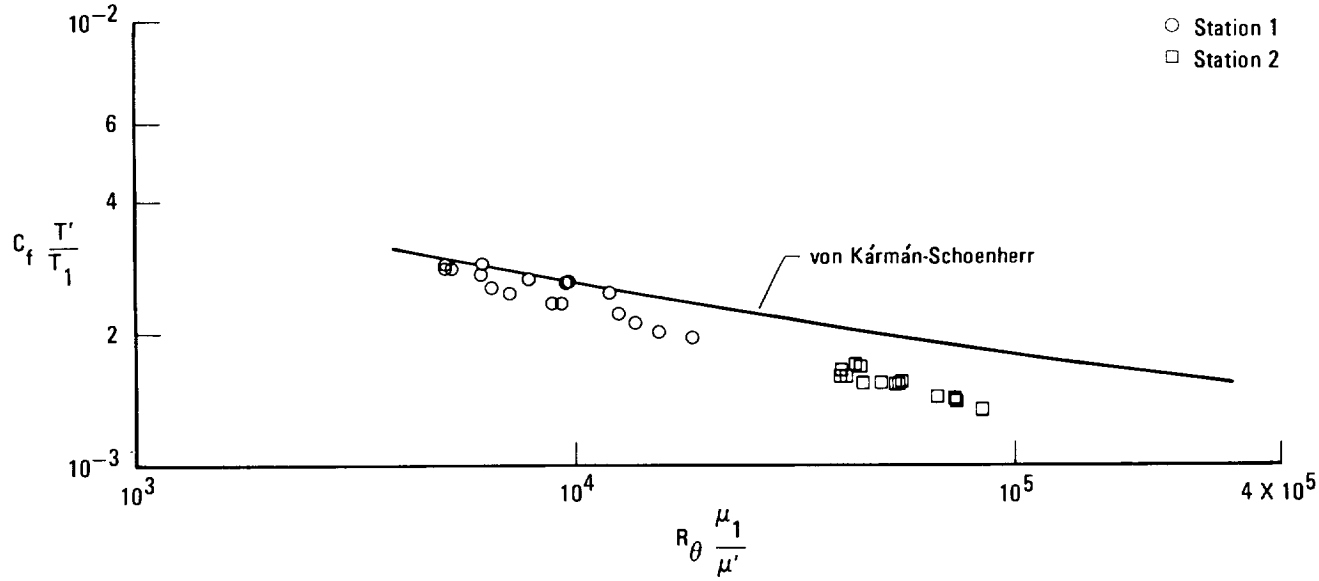

(b) Reynolds number based on θ, momentum thickness.

Figure 9.—Variation of local skin friction coefficient from the friction force balance as a function of Reynolds number.

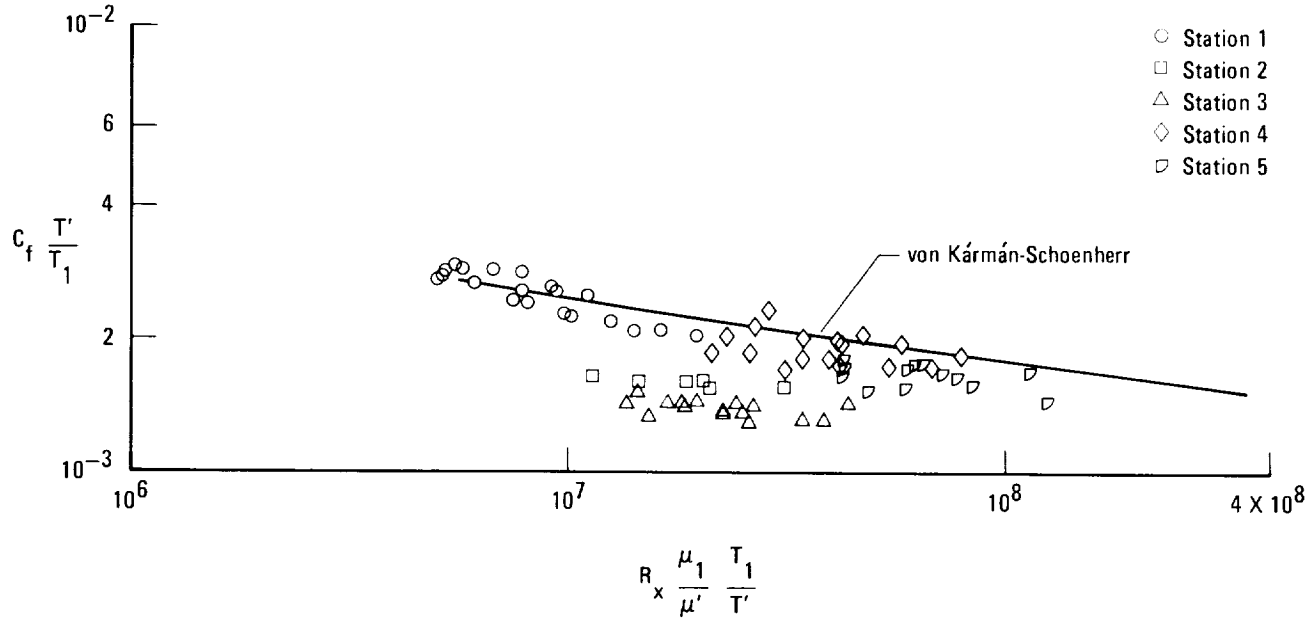

(a) Reynolds number based on x, distance from nose apex.

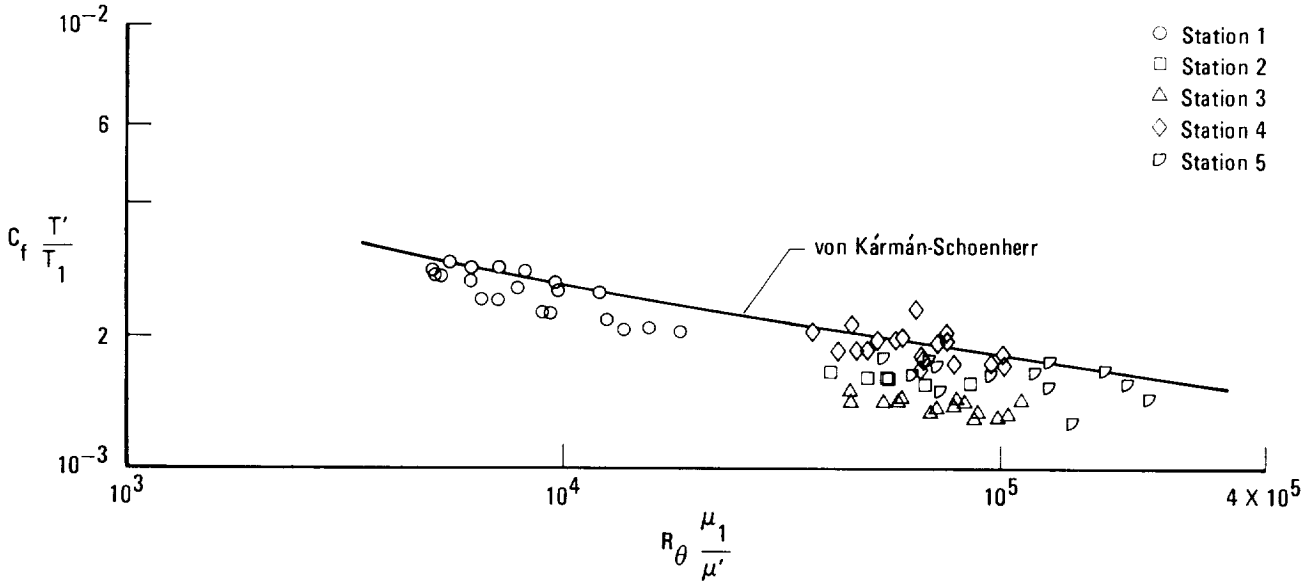

(b) Reynolds number based on θ, momentum thickness.

Figure 10.—Variation of local skin friction coefficient from the Preston probe as a function of Reynolds number.

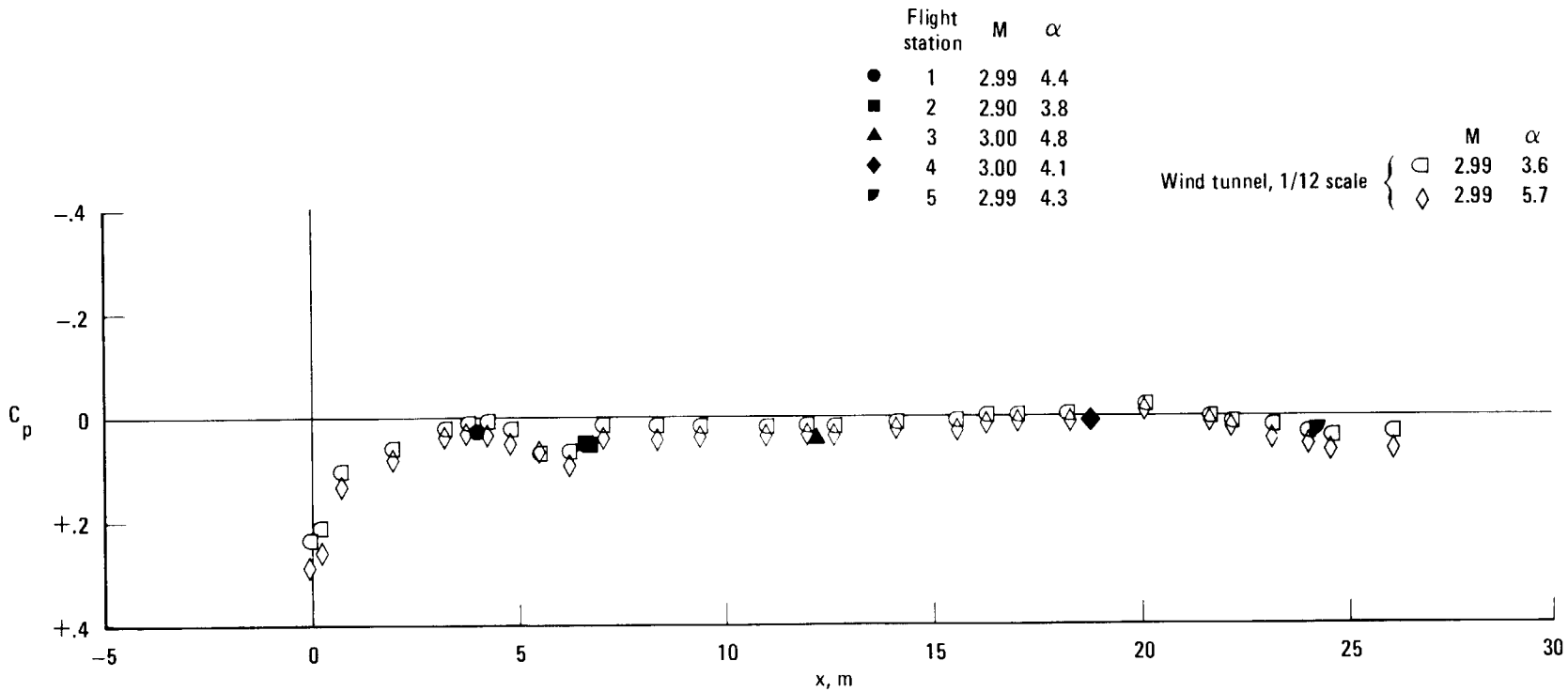

Figure 11.—Flight-measured pressure coefficients along the lower fuselage centerline of the YF-12 airplane and corresponding pressure coefficients from a 1/12-scale model.

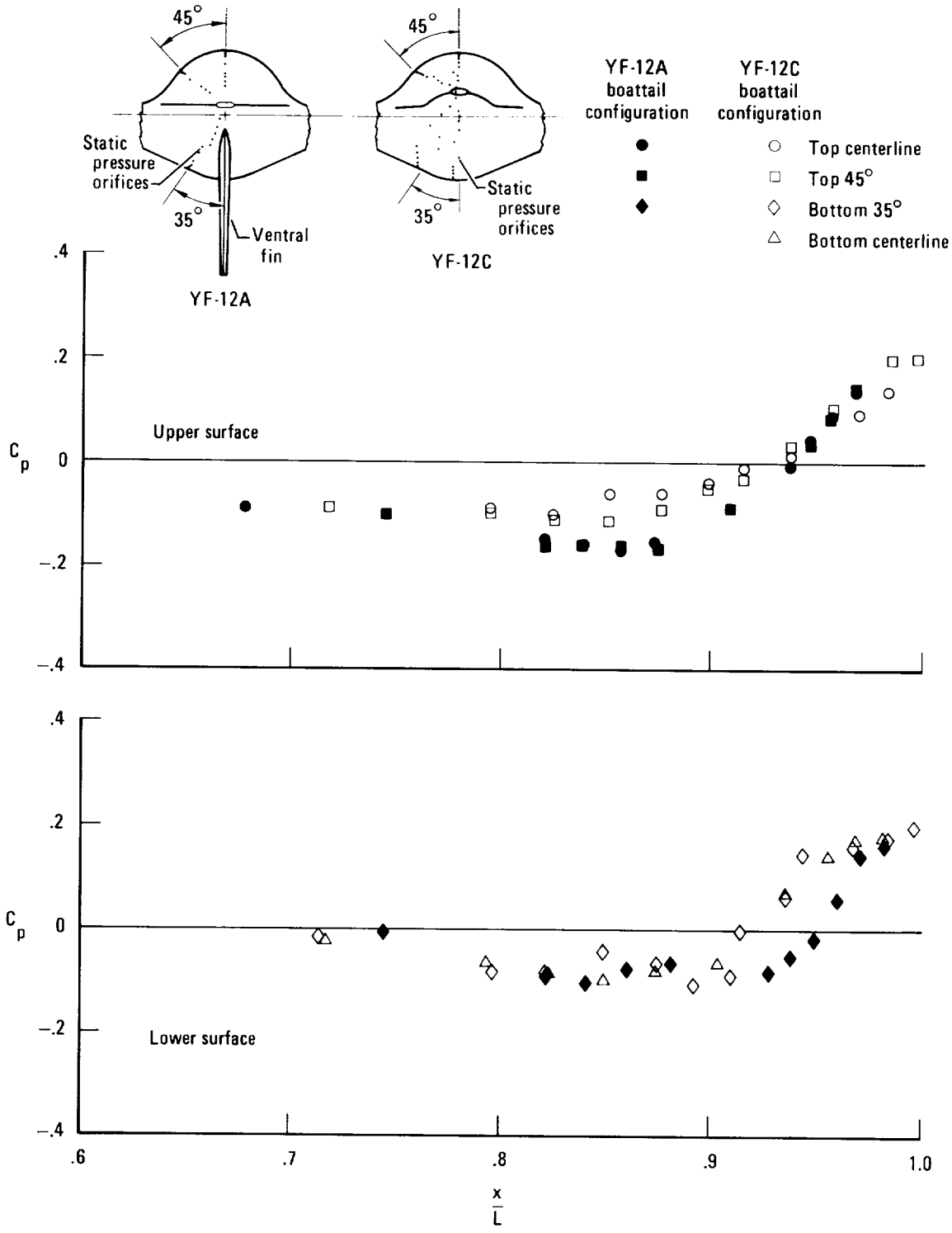

(a) $M \approx 0.7$.

Figure 12.—Pressure distribution on the boattails of the YF-12A and YF-12C airplanes.

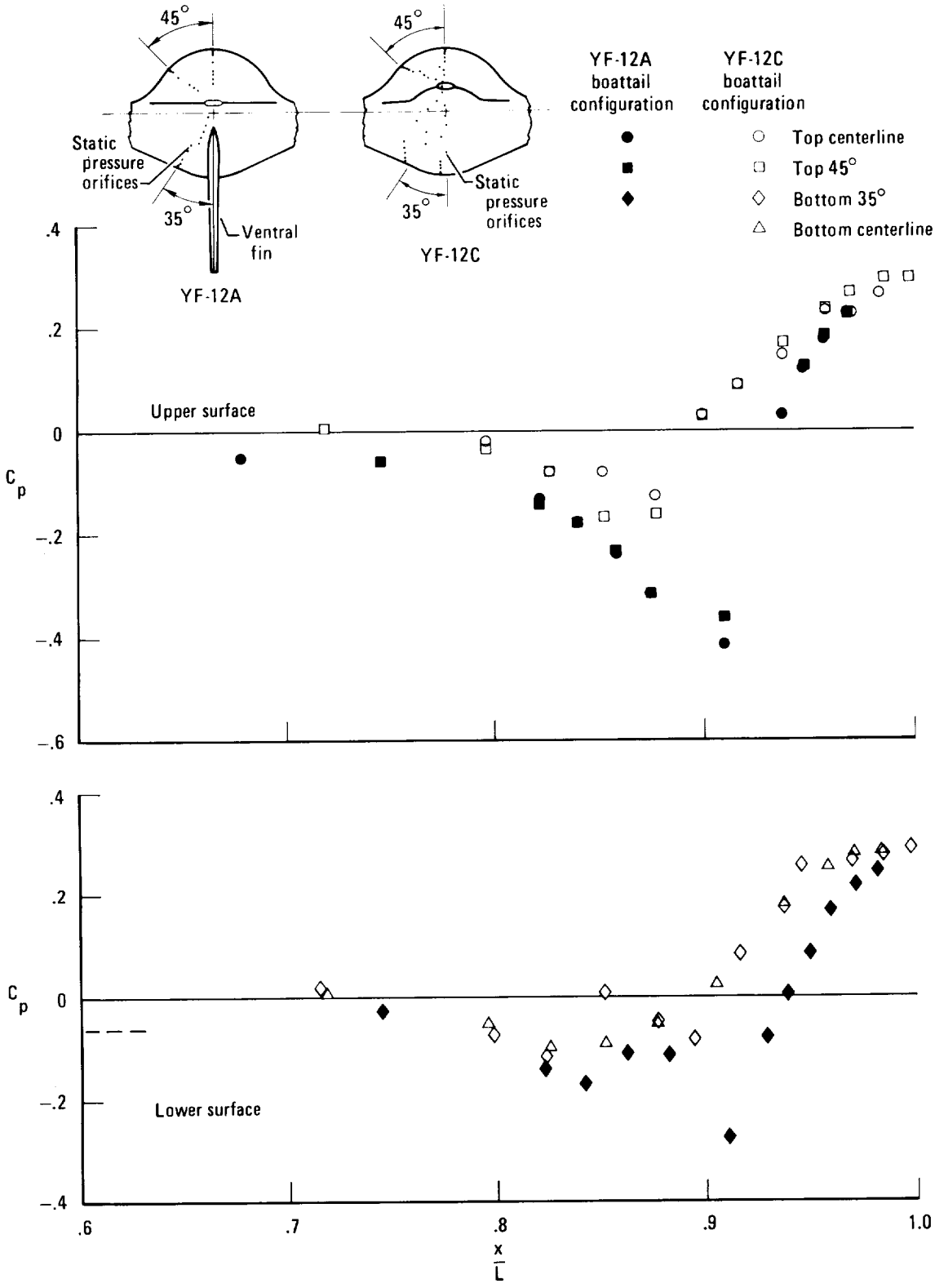

(b) $M \approx 0.96$.

Figure 12.—Continued.

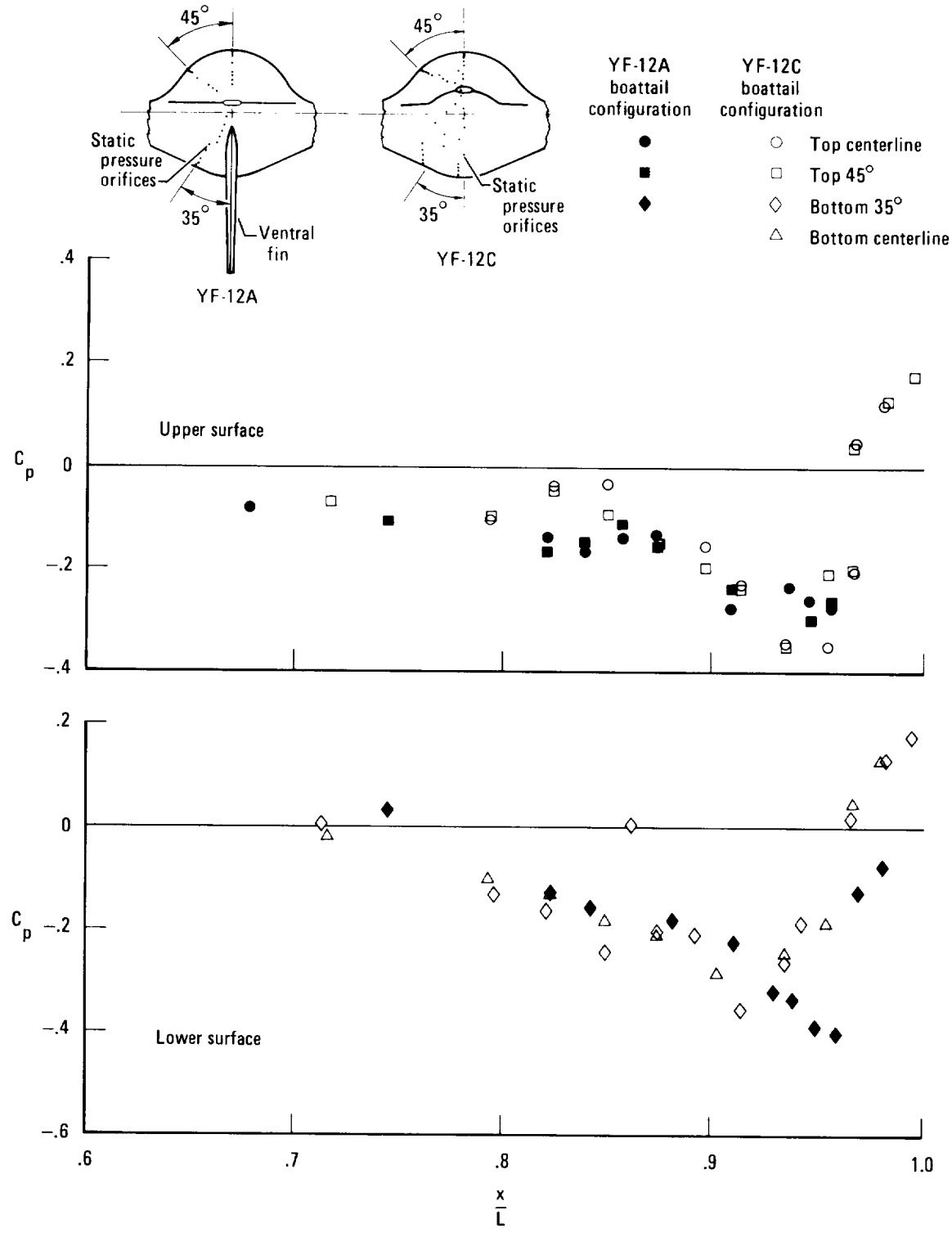

(c) $M \approx 1.12$.

Figure 12.—Continued.

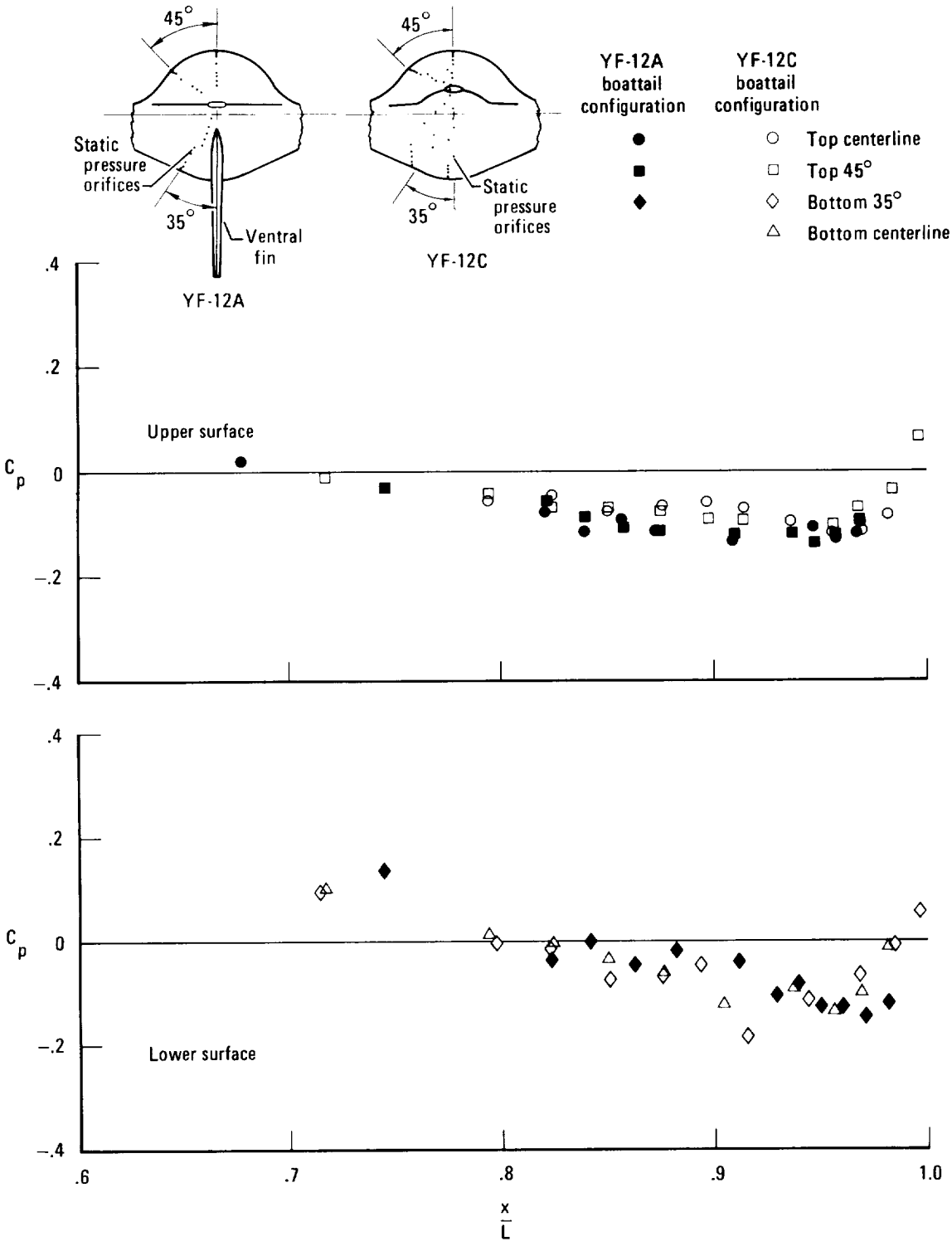

(d) $M \approx 2.0$.

Figure 12.—Continued.

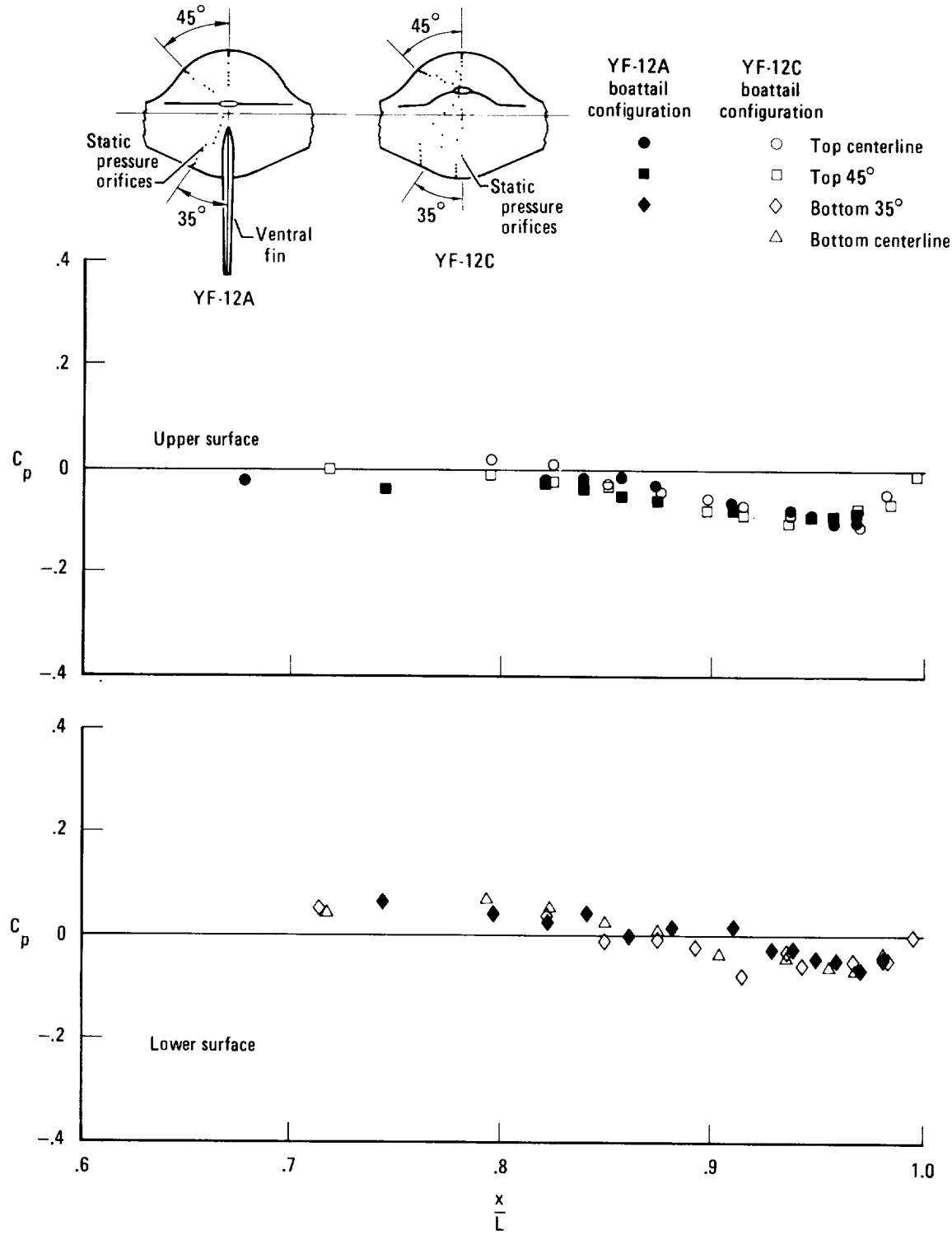

(e) $M \approx 3.0$.

Figure 12.—Concluded.

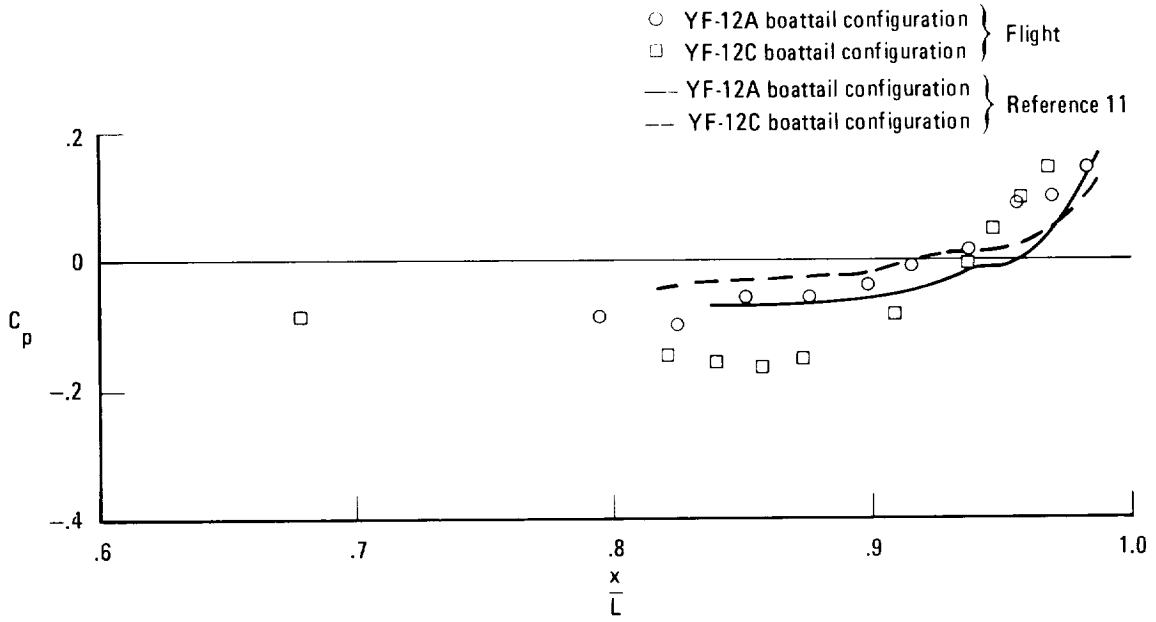

(a) $M \approx 0.7$.

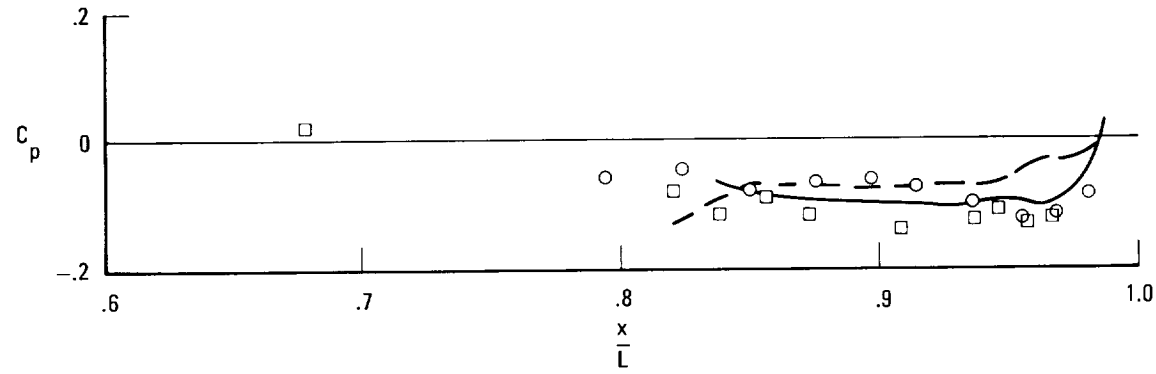

(b) $M \approx 2.0$.

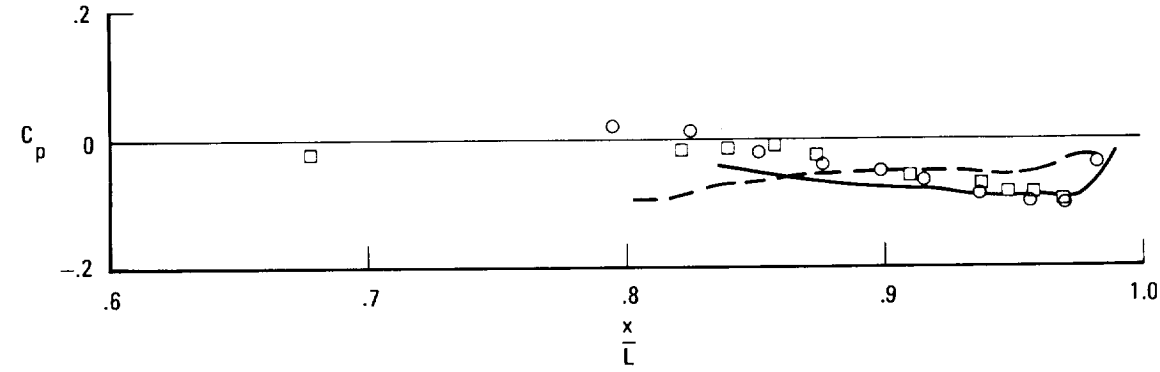

(c) $M \approx 3.0$.

Figure 13.—Comparison of top centerline boattail pressure coefficients for YF-12A and YF-12C configurations with the predictions obtained using the techniques of reference 10.

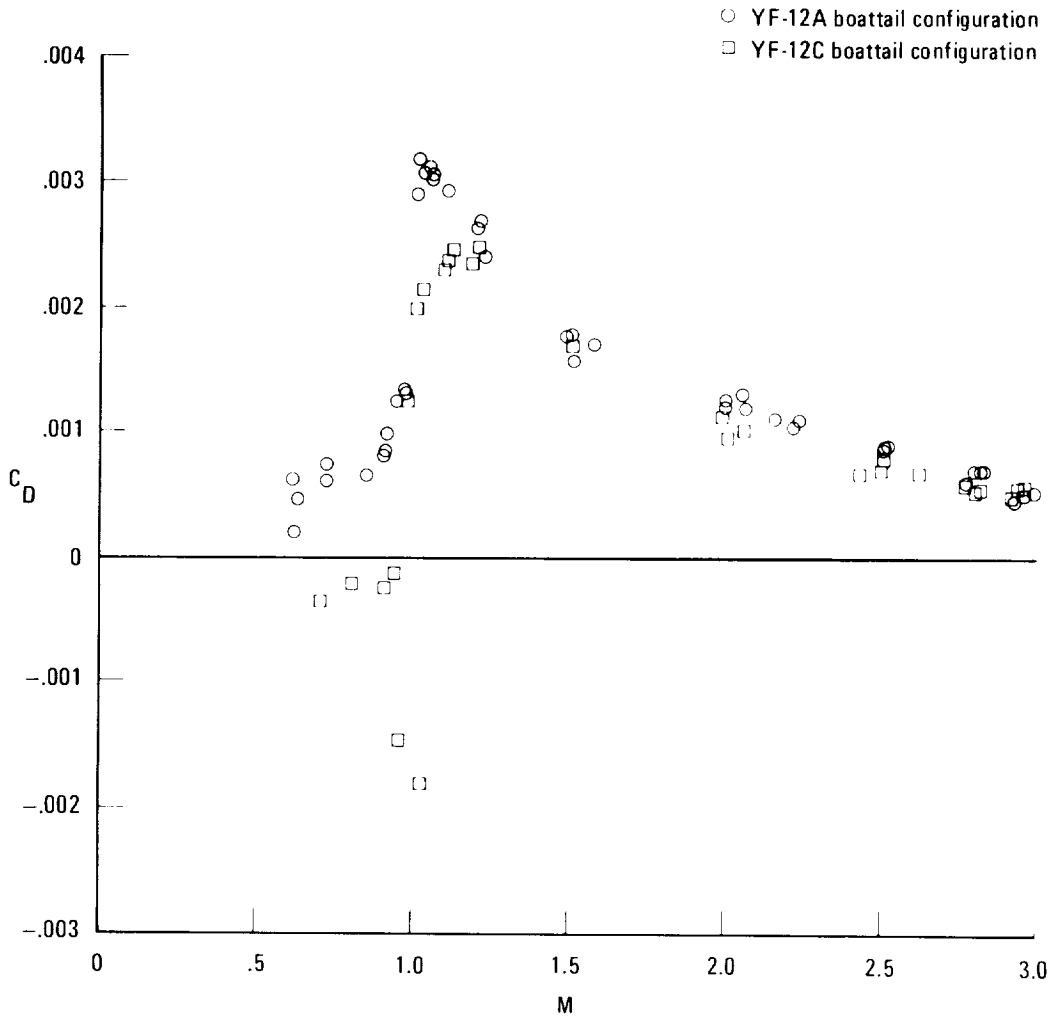

Figure 14.—Variation of boattail pressure drag coefficients as a function of Mach number.